Int J Clin Exp Med 2017;10(1):307-315
www.ijcem.com /ISSN:1940-5901/IJCEM0041080

*Original Article*

# Three-dimensional finite element stress analysis of uneven-threaded ti dental implant

Xingchao Li, Fusheng Dong

*Department of Oral and Maxillofacial Surgery, Stomatology Hospital of Hebei Medical University, Shijiazhuang 050017, China*

Received October 1, 2016; Accepted November 3, 2016; Epub January 15, 2017; Published January 30, 2017

**Abstract:** This study aims to investigate the influence of different neck structures on implant stress distribution. A computer-aided design (CAD) mandibular model based on adult mandibular computed tomography (CT) information was first established, and then used to create a mandibular model and a related mandibular implant model by using Solidworks. The implant was then fitted to the mandibular first molar. Four neck-type implants, i.e., uniform-threaded implant (UT), wide-neck implant (WN), implant with single-microthreaded neck (SMN), and implant with double-microthreaded neck (DMN), received axial 100-N, horizontal 50-N, and oblique 100-N loads, by using the Ansys Workbench software; the Von Mises equivalent stress (ES) and maximum principal stress (MPS) in different implant groups were then compared. Axial 100-N load: the maximum ES in the cortical bone area (CB-MES, MPa) was 46.58, 35.25, 20.98, and 58.01 in UT, WN, SMN, and DMN respectively; the MPS at the superior edge of cortical bone (CB-MPS, MPa) was 0.97, 0.89, 0.79, and 1.22 in the same four groups respectively. Horizontal 50-N load: CB-MES was 53.21, 41.93, 36.95, and 64.18 in UT, WN, SMN, and DMN respectively; CB-MPS was 41.77, 39.61, 29.67, and 46.99 in the same four groups respectively. Oblique 100-N load: CB-MES was 49.37, 47.78, 34.02, and 78.52 in UT, WN, SMN, and DMN respectively; CB-MPS was 29.35, 21.28, 15.34, and 34.69 in the same four groups respectively. CB-MES and CB-MPS of SMN were the smallest.

**Keywords:** Dental implant, uneven thread, microthread, wide neck, 3D finite element

## Introduction

Thread shapes play very important roles in biomechanical optimization designs of implants; some thread parameters such as height, width, vertex angle, pitch, and helix angle determine thread function, and can largely affect the biomechanical transmission of the implant [1]. Stress mainly concentrates in the cortical and cancellous bone, and is located at the top and bottom area of the implantation fossa. The stress concentration at the top cortical bone is due to its larger elastic modulus, and is also related to the direct contact of implant top with the prosthetic replacement [2]. Blaszczyszyn et al. [3] reported that an immediate-loading implant with microthreaded neck structures (IMTN) exhibited better results 1 year later than those without a microthreaded neck. Implants with long smooth necks would cause the loss of peri-neck bones, but IMTN could change the direction of force transmission at the sites with highly concentrated neck-stress and increase the contact area with bones, compared to a relatively smooth neck, thus slowing the resorption of neck marginal bones [4-7]. Hudieb et al. [8] reported that for IMTN, maximum principal stress (MPS) was transmitted along the lower side perpendicular to the microthread, regardless of the loading angle; however, for implants with a smooth neck, the main stress would be affected by the loading direction, thus easily producing great shear force. Meric et al. [9] studied the mechanics of a fixed denture with a microthreaded and non-microthreaded neck, and found that the former could reduce the stress concentration on the cortical bone area and implant-abutment complex, thus slowing bone resorption. Amid et al. [10] also reported that IMTN could reduce the stress at the neck marginal bones, thus increasing the stress on the cancellous bone, which is conducive to preserving the marginal bone levels. IMTN could alter the stress conduction patterns on the bone interface and increase the surface area of the implant, whose effects in delaying the bone

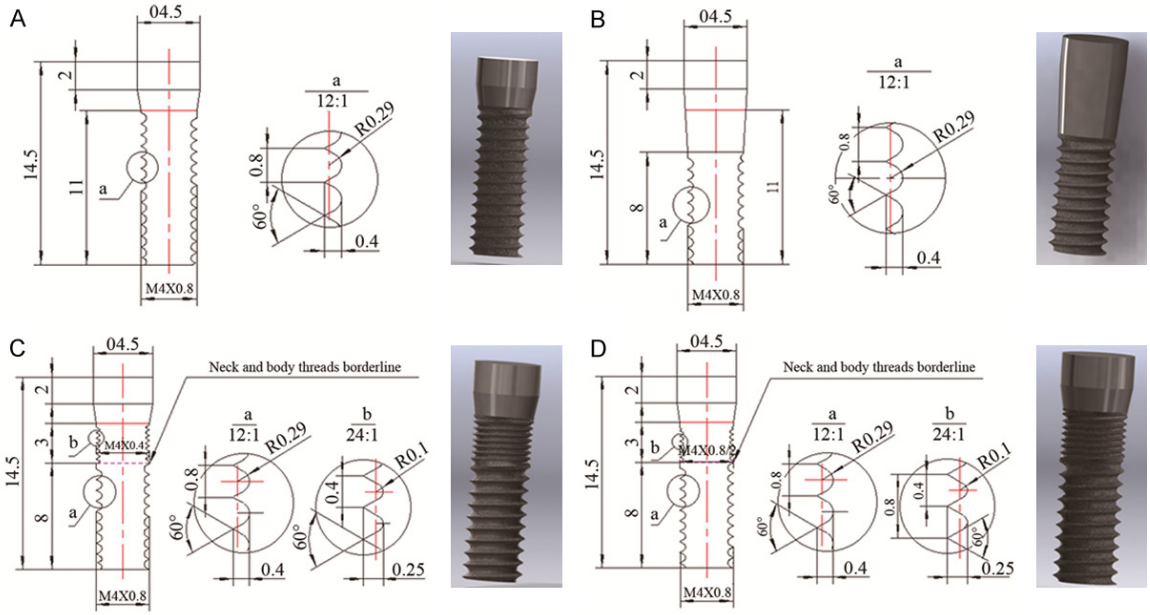


**Figure 1.** Geometric parameters of different IMTN.

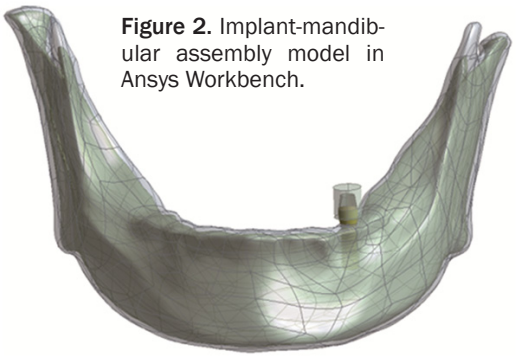

**Figure 2.** Implant-mandibular assembly model in Ansys Workbench.

resorption have already been demonstrated. However, the influence of the IMTN form, parameters, and its combination with a lower main thread on the stress distribution of cortical bone has not been reported. This study focused on comparing the impact of different IMTN designs and their combinations on stress distribution, aiming to provide a theoretical basis for clinically designing and selecting optimal IMTN parameters.

## Materials and methods

### *Implant*

Four cylindrical implants with different thread forms were selected, with diameter 4.0 mm and length 14.5 mm (**Figure 1**).

Thread parameters of the uniform-threaded implant (UT): length 11 mm, apex angle 60°, depth 0.40 mm, pitch 0.8 mm.

Thread parameters of the wide-neck implant (WN): length 8 mm, apex angle 60°, depth 0.40 mm, pitch 0.8 mm.

Thread parameters of the implant with single-microthreaded neck (SMN): length 11 mm: lower part 8 mm, apex angle 60°, depth 0.40 mm, pitch 0.8 mm; upper part 3 mm, apex angle 60°, depth 0.25 mm, pitch 0.4 mm.

Thread parameters of the implant with double-microthreaded neck (DMN): length 11 mm: lower part 8 mm, apex angle 60°, depth 0.40 mm, pitch 0.8 mm; upper part 3 mm (dual parallel microthread), apex angle 60°, depth 0.25 mm, tooth pitch 0.4 mm, pitch 0.8 mm.

### *Mandibular model*

*Preliminary modeling:* 300 images containing a complete mandible were selected from the Digital Imaging and Communications in Medicine (DICOM) files of entire cranial computed tomography (CT) scans, and a corresponding new project was established in Mimics 16.0 (Materialise, Belgium). According to the gray values of the CT images, the bony part was extracted with the threshold region determined

**Table 1.** Nodes and units of the model

| Group | Nodes of the overall model | Units of the overall model | Nodes at the implant | Units at the implant |
|---|---|---|---|---|
| UT | 642184 | 428067 | 11800 | 6398 |
| WN | 635043 | 427232 | 12291 | 6776 |
| SMN | 480990 | 320691 | 11353 | 6016 |
| DMN | 754098 | 433957 | 17817 | 9959 |

Note: UT: Uniform thread implant; WN: Wide neck implant; SMN: Implant with single-microthreaded neck; DMN: Implant with double-microthreaded neck.

**Table 2.** Elastic properties of materials

| Material | Elastic modulus (GPa) | Poisson's ratio | Reference |
|---|---|---|---|
| Cortical bone | 14 | 0.3 | [11] |
| Cancellous bone | 1.37 | 0.31 | [12] |
| Ti | 110 | 0.35 | [13] |
| Porcelain | 68.9 | 0.28 | [14] |

within 98 to 3071 according to the field CT gray levels in the help documentation of Mimics 16.0, and the pixels within this range were placed in the masking materials of the bone to achieve the separation of muscle and bone. The bony masking materials were edited, and an accurate void-free masking model that only included mandible pixels was obtained. The 3-dimensional (3D) model was then automatically calculated by using the intra-masking pixels, and irrational structures were excluded by observing, inspecting, and editing the 3D model. The final generated preliminary 3D geometric model of the mandible was output using the STL format (Standard Template Library).

*Model optimization:* The STL-formatted preliminary 3D geometric model of the mandible was then introduced into Geomagic studio 2013 (Geomagic Inc., USA), appearing as a polygonal surface model; this was followed by preliminary smoothing using several rapid fairing operations. Thereafter, by creating a flow pattern, removing spikes and high refractive edges, relaxing, and local sanding, the polygonal surface performance was further improved. Complex bad surfaces were deleted directly, and the local features were improved by curvature-based filling and hole-bridging operations. Local smooth transition was achieved by removing non-interesting complex features. After examining the polygon qualities and eliminating the defects using the "mesh doctor", a mandibular polygon model was ultimately obtained. The polygon model was then transmitted into the accurate surface stage: first, the contour lines were detected using automatic curvature detection; second, the critical boundaries were artificially enhanced and constrained according to the actual model features; finally, the model was repeatedly revised until reasonable, according to the structures of subsequent patches. After constructing the patches, the surface patch quality was further enhanced by moving the panel vertices, defining and modifying the patches, fitting the contours, relaxing, or other operations, until the mandibular patch model was ultimately obtained. After creating the mandibular nonuniform rational B-spline surfaces and computer-aided design (CAD) object conversion, the mandibular CAD model was finally obtained.

*Generation of cortical and cancellous bones*

The cortical bone was about 1.5 mm thick. Accordingly, at the Geomagic polygon phase, the model of the interface of mandibular cortical and cancellous bones was obtained by drawing the shell 1.5 mm inward and removing the crossing surface; the above steps were then re-operated step-by-step, so that the cancellous bone CAD model could then be obtained with the interface as the outer contour. The overall mandibular CAD model and the cancellous bone CAD model were then introduced into Solidworks 2015 (Solidworks Co., USA) to obtain the cortical bone model by a Boolean subtraction operation.

*Assembly of implant and mandible*

The 4 types of implants were then fixed at the same place in the mandibular first molar region through translation and rotation, and the axis of the implant was approximately perpendicular to the surface of the mandibular alveolar ridge crest at this place. The mandibular cortical and cancellous bones were then subduced by the implant using the Boolean subtraction operation to achieve accurate thread-fitting between the mandible and the implant. After having determined the implant position,

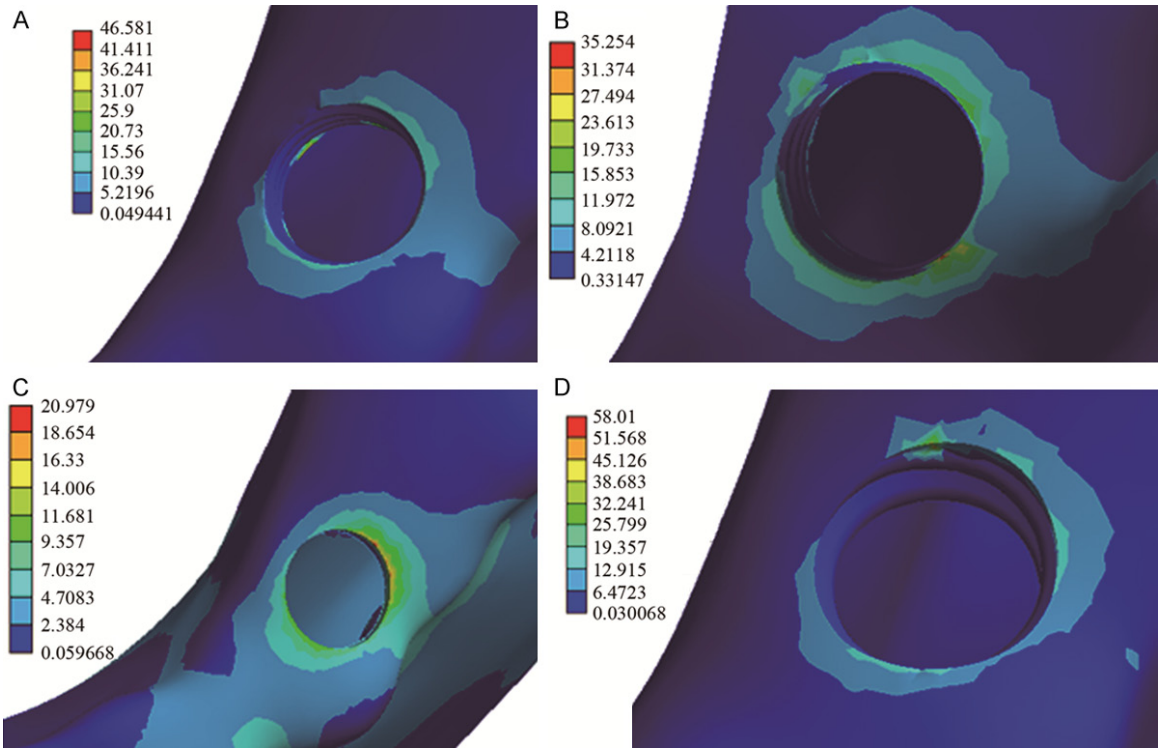


**Figure 3.** Von-Mises ES distribution of peri-cortical bone area under the axial load.

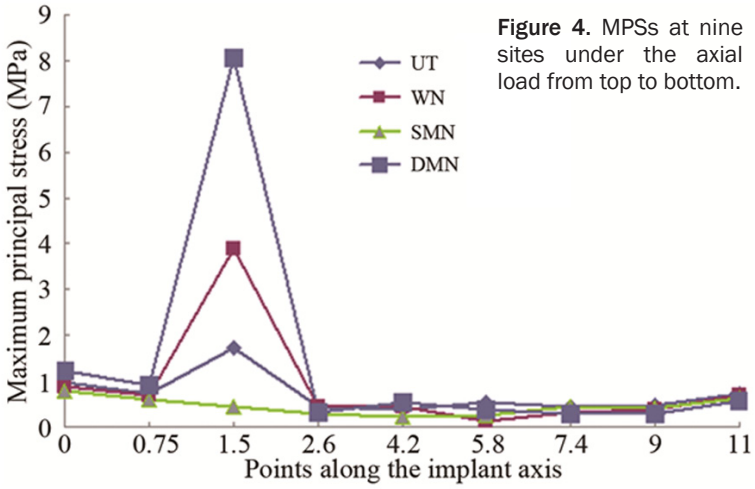


**Figure 4.** MPSs at nine sites under the axial load from top to bottom.

one 3.2-mm high abutment was established on the implant top using Solidworks, on top of which one 2-mm thick ceramic dental prosthetic restoration was then established, followed by importing into the Ansys Workbench 14.5 (Ansys Inc., USA) with the SAT format (**Figure 2**).

*Meshing*

The hexahedron-based and tetrahedron-supplemented automatic meshing method was used, with a unit size of approximately 0.5 mm, and the densities of the nodes and units at and around the implant were properly increased (**Table 1**).

*Material properties*

All the materials used in this study were assumed to be homogeneous and isotropic linear elastic materials, with small elastic deformation; the implant and abutment were Ti and the prosthetic materials were porcelain (**Table 2**).

*Constraints*

The degree of freedom of all the nodes along the top of the bilateral mandibular condyle was set as a rigid constraint to prevent the displacement of the mandible; the implant and the bone tissues were set at 100% of osseointegration, and these 2 materials did not show relative sliding under loads; the ceramic restoration and the implant were set as the immobilized contact.

*Loading conditions*

Uniformly distributed loads under the following 3 conditions were applied onto the implants: axial 100-N load, horizontal 50-N load from the buccal side to the tongue, and oblique 100-N load from the buccal side downward to the tongue and forming a 30° angle with the implant axis.

*Evaluation indexes*

The observation indexes were the Von Mises equivalent stress (ES) and MPS, and the distribution Von Mises ES nephograms of the 4 implant-mandibular models under the 3 loading conditions were then obtained; MPS at 9 sites from the superior border of the cortical bone to the implant bottom on the implant-bone interface was then measured.

## Results

*Axial 100-N load*

Maximum ES in the cortical bone area (**Figure 3**): The maximum ES in the cortical bone area in UT, WN, SMN, and DMN was 46.58 MPa, 35.25 MPa, 20.98 MPa, and 58.01 MPa, respectively.

MPS (**Figure 4**): MPS at the superior border of the cortical bone was 0.97 MPa, 0.89 MPa, 0.79 MPa, and 1.22 MPa, respectively; MPS at the junction of cortical and cancellous bones was 1.72 MPa, 3.89 MPa, 0.45 MPa, and 8.07 MPa, respectively; MPS at the end of the implant was 0.73 MPa, 0.67 MPa, 0.64 MPa, and 0.57 MPa, respectively.

MPS at the mid-point of the cancellous bone area was relatively lower.

*Horizontal 50-N load*

Maximum ES in the cortical bone area (**Figure 5**): The maximum ES in the cortical bone area in UT, WN, SMN, and DMN was 53.21 MPa, 41.93 MPa, 36.95 MPa, and 64.18 MPa, respectively.

MPS (**Figure 6**): MPS at the superior border of the cortical bone was 41.77 MPa, 39.61 MPa, 29.67 MPa, and 46.99 MPa, respectively; MPS at the junction of cortical and cancellous bones was 9.45 MPa, 2.80 MPa, 1.73 MPa, and 9.49 MPa, respectively; MPS at the end of the implant was 0.07 MPa, 0.09 MPa, 0.15 MPa, and 0.26 MPa, respectively.

MPS in the cortical bone area was relatively higher.

*Oblique 100-N load*

Maximum ES in the cortical bone area (**Figure 7**): The maximum ES in the cortical bone area in UT, WN, SMN, and DMN was 49.37 MPa, 47.78 MPa, 34.02 MPa, and 78.52 MPa, respectively.

MPS (**Figure 8**): MPS at the superior border of the cortical bone was 29.35 MPa, 21.28 MPa, 15.34 MPa, and 34.69 MPa, respectively; MPS at the junction of cortical and cancellous bones was 3.50 MPa, 2.71 MPa, 0.97 MPa, and 8.58 MPa, respectively; MPS at the end of the implant was 0.16 MPa, 0.11 MPa, 0.15 MPa, and 0.10 MPa, respectively.

MPS in the cortical bone area was relatively higher.

## Discussion

The results of this study indicated that different neck morphologies of a cylindrical implant with V-shaped microthread would affect the stress distribution on the implant-bone interface; under the 3 loads conditions, the overall stress concentration areas were all located at the cortical bone area and the apical part around the implant neck, consistent with previous findings [2]. Under 3 experimental loads, the maximum ES in the cortical bone area and MPS at the superior border of the cortical bone exhibited the smallest values in SMN, followed by WN, UT, and DMN, consistent with previous studies. Schrotenboer et al. [15] also confirmed that implants with microthreaded neck exhibited smaller load on the cortical bone than those with smooth neck when horizontal and oblique loads were applied. Rahimi et al. [16] reported that the microthreaded neck could spread the stress of the implant, in the manner of compressive stress, to surrounding bones via the thread slopes, thus changing the conduction form of loads. Abrahamsson and others also showed that the microthreaded neck could maintain the marginal bone level, thus exhibiting better clinical results than the implants with a smooth neck [17-20].

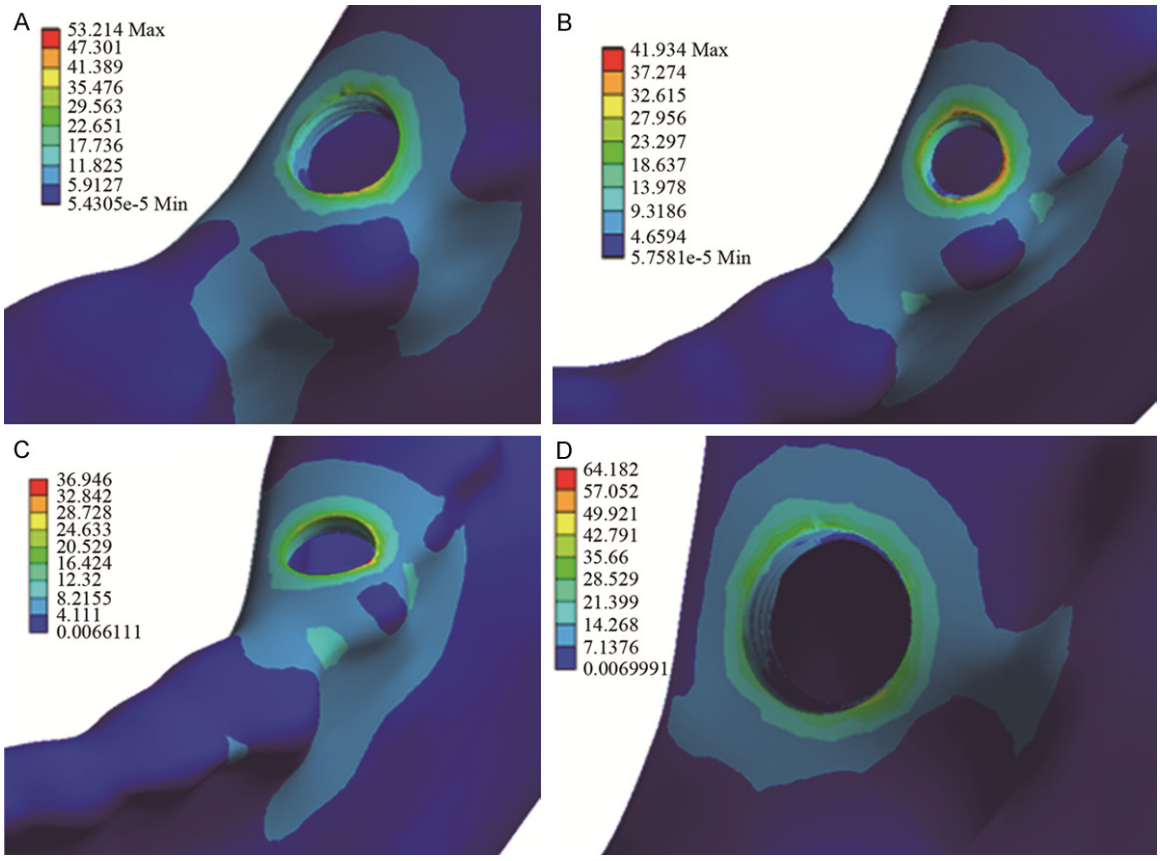


**Figure 5.** Von-Mises ES distribution of peri-cortical bone area under the horizontal load.

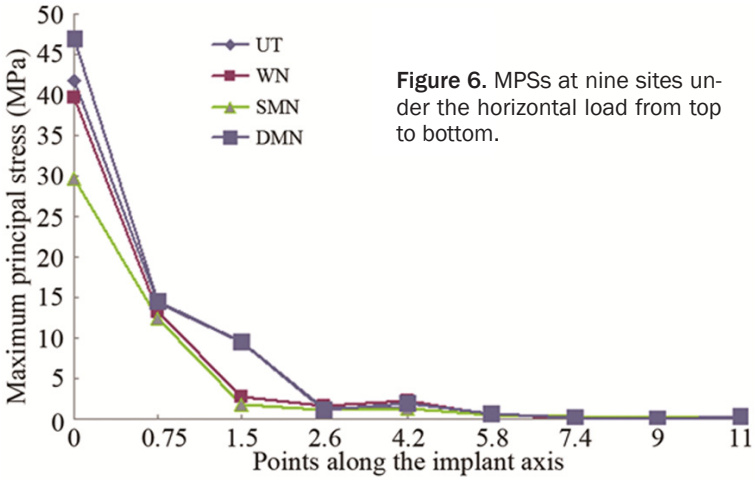


**Figure 6.** MPSs at nine sites under the horizontal load from top to bottom.

The impact of a microthreaded neck on the stress was associated with a number of assumptions: Song et al. [21] reported that the position of the microthread had great impact on maintaining the bone edge, and that when the thread started 0.5 mm under the implant bone level and was roughly parallel to the bone plane, more bone loss was observed clinically; the possible reason was determined to be the stress concentration at the thread edge. In this study, the microthreads in UT, SMN, and DMN all started from the bone plane in order to achieve better preservation of the marginal bone. The results suggested that the axial load-induced stress was concentrated on the superior edge of cortical bone, on the junction of cortical bone and cancellous bone, and on the bottom of the implant. Von Mises ES and MPS in the cortical bone area of SMN were the smallest, followed by WN, UT, and DMN. SMN exhibited obvious effects in confronting vertical loads, possibly due to its smaller rotation angle, so that the stress conduction direction was changed, thus reducing the shear force. In contrast, DMN exhibited larger neck

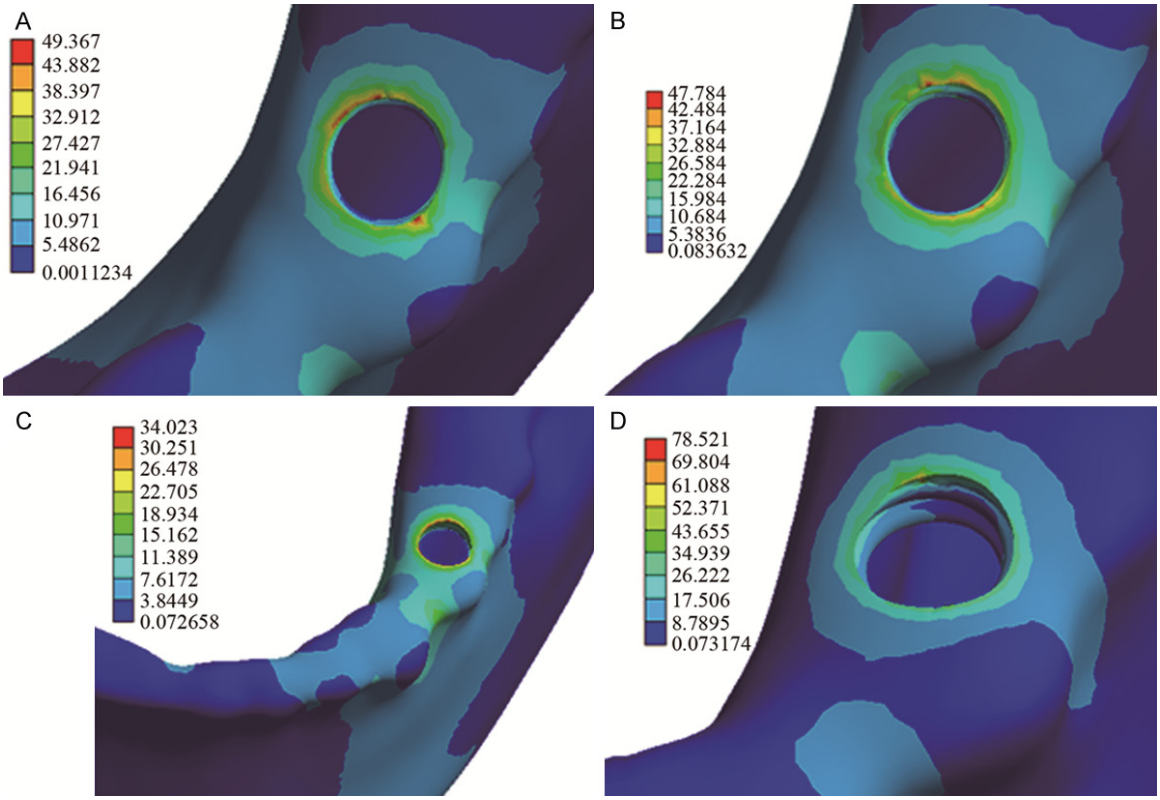


**Figure 7.** Von-Mises ES distribution of peri-cortical bone area under the oblique load.

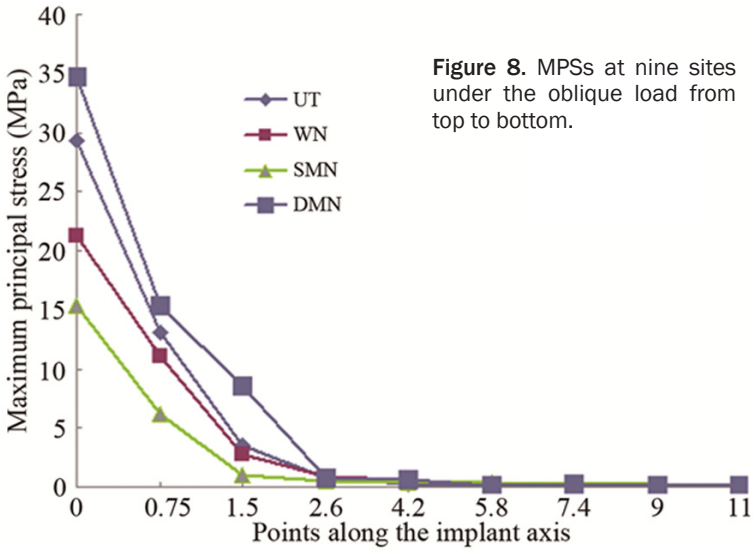


**Figure 8.** MPSs at nine sites under the oblique load from top to bottom.

stress, possibly due to its larger microthreaded rotation angle, which led to worse vertical-load confronting ability, consistent with the research of Herekar et al. [22]. In addition, the surface area of the implant with microthreaded neck (SMN and DMN) was increased by about 15.40% and 45.52%, compared to UT and WN respectively, which might reduce the stress concentration at the neck. When subjected to horizontal and oblique loads, the stress concentrated in the cortical bone area and the stress on the superior edge of the cortical bone were the greatest, and descended in order. In the cortical bone area, SMN exhibited the smallest Von Mises ES and MPS, followed by WN, UT, and DMN. The obvious effects of anti-horizontal and anti-oblique loads on SMN possibly can be explained by the fact that the smaller rotation angle changed the stress conduction direction, and that the microthread increased the contact area with the bone. WN exhibited smaller stress in the cortical bone area than UT and DMN; this might have resulted from the increased neck diame-

ter of the implant, which had greater impact on the stress distribution induced by lateral loads.

This study was based on the assumptions of continuous, homogeneous, isotropic, linear elastic, and small deformations; these assumptions would only simplify the calculation rather than affect the comparability of the results; therefore, the steps of integrating, calculating, and analyzing different nodes had small error probabilities. Meanwhile, a number of confounding factors could also be excluded. During the study, some simplifications and assumptions were also performed: based on an average chewing force in Chinese of 30 N-300 N, the directions of biting force were simplified into axial 100-N, horizontal 100-N, and oblique 50-N loads. In addition, the shape of the dental prosthetic restoration was simplified into a nonanatomic occlusal cylinder, which also differed from clinical reality; however, these did not affect the measurements and data analysis targeting the study purposes because all the models were prepared under the same assumptions and simplified conditions; thus, the results were comparable.

The assumptions could also affect the results of finite element analysis, but the effects of the optimized microthread implant neck, including the distribution position, shape, parameters, rotation angle, and combination features with the main thread, on the stress distribution at the implant-bone interface had been initially confirmed. Further studies should target primary stability, spin-out torque, fatigue characteristics, clinical preservative effects on the marginal bone, etc., thus providing a complete basis for optimizing the design of the neck thread.

## Conclusions

Different neck forms of cylindrical implants with V-shaped microthreads affected implant-bone interface stress and stress distribution; the overall stress concentration area was located at the cortical bone area and the apical part around the implant neck. SMN with the same thread form significantly reduced the Von Mises ES and MPS in the cortical bone area when axial, horizontal, and oblique loads were applied.

## Acknowledgements

This study was funded by the major medical research projects of Hebei (zd2013076).

## Disclosure of conflict of interest

None.

**Address correspondence to:** Fusheng Dong, Department of Oral and Maxillofacial Surgery, Stomatology Hospital of Hebei Medical University, No. 383 Zhongshan Road, Changan District, Shijiazhuang 050017, China. Tel: +86 311 86265514; Fax: +86 311 86265748; E-mail: fushengdongdoc@163.com

## References

[1] Hansson S and Werke M. The implant thread as a retention element in cortical bone: the effect of thread size and thread profile: a finite element study. J Biomech 2003; 36: 1247-1258.

[2] Hudieb M and Kasugai S. Biomechanical effect of crestal bone osteoplasty before implant placement: a three-dimensional finite element analysis. Int J Oral Maxillofac Surg 2011; 40: 200-206.

[3] Blaszczyszyn A, Heinemann F, Gedrange T, Kawala B, Gerber H and Dominiak M. Immediate loading of an implant with fine threaded neck-bone resorption and clinical outcome of single tooth restorations in the maxilla. Biomed Tech (Berl) 2012; 57: 3-9.

[4] Chowdhary R, Jimbo R, Thomsen CS, Carlsson L and Wennerberg A. The osseointegration stimulatory effect of macrogeometry-modified implants: a study in the rabbit. Clin Oral Implants Res 2014; 25: 1051-1055.

[5] Yun HJ, Park JC, Yun JH, Jung UW, Kim CS, Choi SH and Cho KS. A short-term clinical study of marginal bone level change around microthreaded and platform-switched implants. J Periodontal Implant Sci 2011; 41: 211-217.

[6] Choi KS, Park SH, Lee JH, Jeon YC, Yun MJ and Jeong CM. Stress distribution scalloped implants with different microthread and connection configurations using three-dimensional finite element analysis. Int J Oral Maxillofac Implants 2012; 27: 29-38.

[7] Calvo-Guirado JL, Gómez-Moreno G, Aguilar-Salvatierra A, Guardia J, Delgado-Ruiz RA and Romanos GE. Marginal bone loss evaluation around immediate non-occlusal microthreaded implants placed in fresh extraction sockets in the maxilla: a 3-year study. Clin Oral Implants Res 2015; 26: 761-767.

[8] Hudieb MI, Wakabayashi N and Kasugai S. Magnitude and direction of mechanical stress at the osseointegrated interface of the microthread implant. J Periodontol 2011; 82: 1061-1070.

[9] Meric G, Erkmen E, Kurt A, Eser A and Ozden AU. Biomechanical comparison of two different collar structured implants supporting 3-unit

fixed partial denture: a 3-D FEM study. Acta Odontol Scand 2012; 70: 61-71.
[10] Amid R, Raoofi S, Kadkhodazadeh M, Movahhedi MR and Khademi M. Effect of microthread design of dental implants on stress and strain patterns: a three-dimensional finite element analysis. Biomed Tech (Berl) 2013; 58: 457-467.
[11] Cook SD, Klawitter JJ and Weinstein AM. A model for the implant-bone interface characteristics of porous dental implants. J Dent Res 1982; 61: 1006-1009.
[12] Borchers L and Reichart P. Three-dimensional stress distribution around a dental implant at different stages of interface development. J Dent Res 1983; 62: 155-159.
[13] Colling EW. The physical metallurgy of titamium alloys. American Society for Metals, Ohio: Metals Park; 1984. pp. 53-78.
[14] Lewinstein I, Banks-Sills L and Eliasi R. Finite element analysis of a new system (IL) for supporting an implant-retained cantilever prosthesis. Int J Oral Maxillofac Implants 1995; 10: 355-366.
[15] Schrotenboer J, Tsao YP, Kinariwala V and Wang HL. Effect of microthreads and platform switching on crestal bone stress levels: a finite element analysis. J Periodontol 2008; 79: 2166-2172.
[16] Rahimi A, Bourauel C, Jager A, Gedrange T and Heinemann F. Load transfer by fine threading the implant neck--a FEM study. J Physiol Pharmacol 2009; 60: 107-112.
[17] Almeida EO, Freitas Júnior AC, Bonfante EA, Rocha EP, Silva NR and Coelho PG. Effect of microthread presence and restoration design (screw versus cemented) in dental implant reliability and failure modes. Clin Oral Implants Res 2013; 24: 191-196.
[18] Park YS, Lee SP, Han CH, Kwon JH and Jung YC. The microtomographic evaluation of marginal bone resorption of immediately loaded scalloped design implant with various microthread configurations in canine mandible: pilot study. J Oral Implantol 2010; 36: 357-362.
[19] Abrahamsson I and Berglundh T. Tissue characteristics at microthreaded implants: an experimental study in dogs. Clin implant Dent Relat Res 2006; 8: 107-113.
[20] Lee DW, Choi YS, Park KH, Kim CS and Moon IS. Effect of microthread on the maintenance of marginal bone level: a 3-year prospective study. Clin Oral Implants Res 2007; 18: 465-470.
[21] Song DW, Lee DW, Kim CK, Park KH and Moon IS. Comparative analysis of periimplant marginal bone loss based on microthread location: a 1-year prospective study after loading. J Periodontol 2009; 80: 1937-1944.
[22] Herekar MG, Patil VN, Mulani SS, Sethi M and Padhye O. The influence of thread geometry on biomechanical load transfer to bone: A finite element analysis comparing two implant thread designs. Dent Res J (Isfahan) 2014; 11: 489-494.